This article has been accepted for publication in a future issue of this journal, but has not been fully edited. Content may change prior to final publication. Citation information: DOI 10.1109/TPEL.2019.2909532, IEEE Transactions on Power Electronics

An Enhanced Control System for Single-Phase Inverters Interfaced with Weak and Distorted Grids

Sushil Silwal, *Student Member, IEEE*, Seyedfoad Taghizadeh, *Student Member, IEEE*, Masoud Karimi-Ghartemani, *Senior Member, IEEE*, M. J. Hossain, *Senior Member, IEEE*, and Masoud Davari, *Member, IEEE*

***Abstract*—This paper presents an enhanced current controller for improving the performance of a class of single-phase grid-connected inverters operating in weak and distorted grid conditions. An inverter designed to operate at normal (strong or stiff and clean) grid conditions may not perform satisfactorily during weak and distorted grid conditions. One major reason is the interfering dynamics of the synchronization or phase-locked loop (PLL). This paper proposes an enhanced control structure for a popular class of single-phase inverters to address this problem. The proposed idea is to include the PLL state variables into the main inverter controller thereby minimizing the undesirable interactions of the PLL with the other components. A method for optimally designing the controller gains is also proposed. Compared to the conventional one, the proposed controller is shown to have a more robust performance over a substantially wider range of weak and distorted grid conditions. Extensive simulation and experimental results are presented to validate the proposed controls.**

***Index Terms*—Weak grid conditions, grid distortions, grid-connected inverters, distributed generation, phase-locked loop.**

I. Introduction

Distributed energy resource (DER) units including generation, storage and controllable load entities are increasingly connected to the grid using power electronic converters. These converters process and control the power exchange between two sides of the converter. They need to comply with the standards on grid power quality and ride-through requirements such as [1]–[3]. In addition to those, they should perform robustly against system changes and uncertainties such as voltage and frequency swings and high grid impedances called the weak grid conditions. A weak grid condition is often caused as a result of the high integration of low inertia, fast-acting DERs at numerous locations at the distribution level [4]. A microgrid, which includes a limited number of DER units, is an example of a weak grid. Dynamics of the inverter becomes more complicated when connected to a weak grid and undesirable harmonic injections, oscillations and stability issues arise [5]–[12].

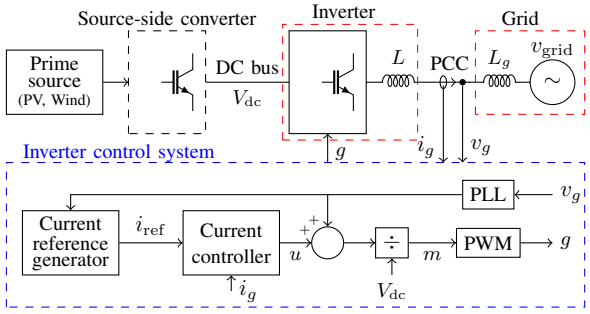

Fig. 1: Schematic diagram of an inverter control system.

DER units are commonly located in dispersed areas where the grid impedance can be high. This can influence the stiffness and quality of the local bus voltage posing interconnection problems which lead to limiting the amount of wind or solar power that can be integrated [13]–[15]. Similarly, [7], [16] show that the dc-link voltage stability degrades with an increase in the power transfer exchange with a weak grid. The work [17] proposes a modified grid voltage feed-forward method using virtual admittance to improve the stability of multi-parallel grid-connected inverters in weak grid conditions. Furthermore, [18] formulates a hierarchical controller for a microgrid to provide coordinated frequency support to a weak grid. It is achieved by adjusting the active power flow in the tie-line as per grid frequency requirements.

The general block diagram of an inverter control system is shown in Fig. 1. This control approach is commonly used in practice. As clearly observed from this figure, the synchronization unit often in the form of a phase-locked loop (PLL) [8], [19]–[23] is critically serving as the interfacing component between the grid voltage and the inverter control system. It is, in general, a nonlinear system which generates a reference for the synchronization and for reference current generation. The effects of the PLL in causing system oscillations during weak grid conditions have been reported in recent publications [5], [8], [12], [23], [24] without offering a comprehensive or systematic solution. In a grid with low short-circuit ratio (SCR), which is an indication of increased grid weakness, designing the PLL is a challenge as higher bandwidths tend to make the system oscillatory and unstable while lower bandwidths degrade its transient speed [24]. Consequently, the interaction of the PLL with other control loops is a dominant factor resulting in instabilities in a weak grid [16]. The work

This work has been partially supported by the U.S. National Science Foundation grant ECCS-EPCN awards #1808368 and #1808279.

Sushil Silwal and Masoud Karimi-Ghartemani are with the Department of Electrical and Computer Engineering, Mississippi State University, E-mail: ss2821@msstate.edu, karimi@ece.msstate.edu;

Seyedfoad Taghizadeh and M.J. Hossain are with the School of Engineering, Faculty of Science and Engineering, Macquarie University, Australia, E-mail: s.t.taghizadeh@ieee.org, jahangir.hossain@mq.edu.au; and

Masoud Davari is with the Department of Electrical and Computer Engineering, Allen E. Paulson College of Engineering and Computing, Georgia Southern University (Statesboro Campus), Statesboro GA 30460, USA, E-mail: davari@ualberta.ca *and* mdavari@georgiasouthern.edu.

This article has been accepted for publication in a future issue of this journal, but has not been fully edited. Content may change prior to final publication. Citation information: DOI 10.1109/TPEL.2019.2909532, IEEE Transactions on Power Electronics

[12] explains the instability occurred in an islanded microgrid by developing and using a nonlinear model. In the same way, [10] has also investigated the operation of current controlled inverters under weak grid conditions and verified that a large grid impedance can destabilize the control system.

A method is presented in [25] to increase the stability range of a voltage source converter (VSC) type of inverters by introducing a virtual impedance term in the PLL which makes the VSC synchronized to a virtual point with a stronger voltage. The reference [26] shows that the system stability is degraded under weak-grid conditions due to the PLL in a current source converter (CSC). It proposes supplementary controllers integrated to the outermost control loops to mitigate the problem. Separate compensation functions are designed through which voltage and frequency variables of the PLL are filtered and used to modify the current reference. The design stage involves determining several control gains and has been done using linear analysis and root-locus method. The work in [27] shows the adverse impacts of the PLL on the performance of a VSC operating in a high voltage dc (HVDC) system with the weak grid, and utilizes an extra damping term to improve the performance of the power synchronization method of [28] against such conditions. The work in [10] investigates the influence of large inductance on the response and stability of the VSC and verifies controller instability in such conditions. It further states that the interaction between the PLL and the current controller plays a significant role in provoking such instability. All these studies discover that PLL causes significant oscillations or even system instabilities during high impedance or weak grid conditions. Some recommend ways to partially compensate these oscillations but none of them succeeds to efficiently or systematically address the problem.

This paper proposes a new approach to systematically addressing the problem of inverter response instabilities during weak grid conditions. The recently developed linear time-invariant (LTI) model of the enhanced PLL (EPLL)—detailed in [29]—is used to integrate its internal state variables fully into the inverter control system. This makes it possible to design the entire system gains (including the PLL and the current controller) together. The paper also develops an optimal control based method to design the entire system gains. This optimal and integral design reduces the loop interactions between the PLL and other control loops resulting in the mitigation of the oscillations that could cause system instabilities. The proposed method is developed for the both L and LCL type output filters. Significant improvement of the inverter performance in weak grid conditions is confirmed using simulations and experimental tests.

II. Study System

The study system is a 6 kVA single-phase grid-connected inverter. Figure 2 shows the complete block diagram and Fig. 3 shows the single-line diagram of the network. A fixed dc source is connected to the inverter via a dc bus. Since the focus of this paper is on converter output current control during weak grid condition, there is no discussion on maximum power point tracking (MPPT) and voltage control. This fixed dc source is

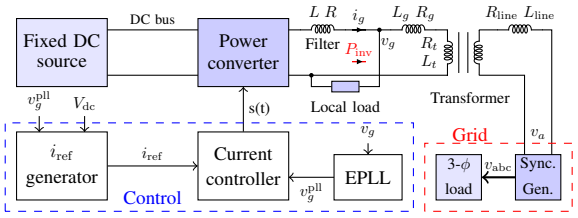

Fig. 2: Study system: Grid-connected inverter

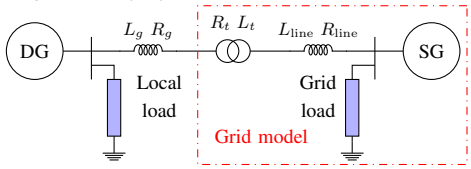

Fig. 3: Single-line diagram of system

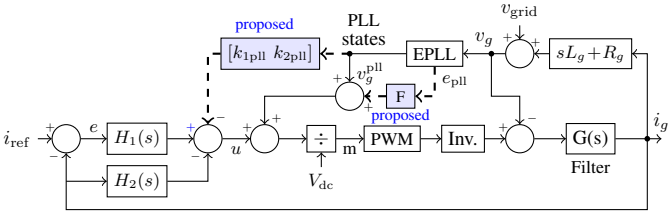

Fig. 4: Conventional and Proposed current controller for single-phase inverters

chosen as an example but the conclusions are generally valid for actual grid-connected DER applications.

The power inverter is connected to the grid at the point of common coupling (PCC) via an L filter whose inductance is chosen such that the peak-to-peak current ripple is less than 10% of the peak rated current. The case of the LCL filter is treated separately in Section IV. For given parameters in Table I and the unipolar PWM, the peak current is $\mathrm{I_p = S_{inv}\sqrt{2}/V_{grid}}$ and thereby $L = 1.3$ mH is selected to limit current ripples to 10% of I_p. The local load is located right after the inverter filter circuit. All the impedances reflecting the real practical effects such as the local grid impedance $Z_g = R_g + j\omega L_g$, the transformer impedance $Z_t = R_t + j\omega L_t$ and the line impedance $Z_{\mathrm{line}} = R_{\mathrm{line}} + j\omega L_{\mathrm{line}}$ are taken into consideration. Furthermore, in order to include the frequency and voltage dynamics of an actual grid as close as possible, a three-phase synchronous generator (SG) based modeling of the grid is used as opposed to simply an ideal voltage source behind an impedance. The inverter is connected to one phase of the three-phase line. The parameters used in the design and simulation of the inverter controller throughout this paper are given in Table I.

III. Current Controller with L-filter

Details of the existing current control approach are shown in Fig. 4. The compensator $H_1(s)$ is for tracking the current reference signal, and consists of a second-order generalized integrator (or resonant controller) tuned to resonate at nominal grid frequency. In the same way, $H_2(s)$ is a proportional gain plus a bank of damped resonant controllers tuned at odd multiples of the grid frequency. However, for the sake of simplicity and making fundamental comparisons, harmonic rejection units in $H_2(s)$ are left out of the scope of this paper.

This article has been accepted for publication in a future issue of this journal, but has not been fully edited. Content may change prior to final publication. Citation information: DOI 10.1109/TPEL.2019.2909532, IEEE Transactions on Power Electronics

TABLE I: Basic system parameters.

Parameter	Symbol	Value
Inverter power rating	S_{inv}	6 kVA
L-filter inductance	L	1.3 mH
L-filter resistance	R	0.1 mΩ
Nominal dc-bus voltage	V_{dc}	600 V
Local load (LL) rating	S_{LL}	4.2 kVA, 0.7 PF
Transformer rating	S_t	10 kVA
Transformer ratio	a	240:7200
Transformer base impedance	Z_t	V_g^2/S_t Ω
Transformer resistance	R_t	$0.02Z_t$ Ω
Transformer inductance	L_t	$0.05Z_t/w_o$ H
Grid inductance	L_g	$0.5-10$ mH
Grid resistance	R_g	$0.3\omega L_g$ Ω
Grid voltage (HV side)	$V_{\text{grid}}^{\text{HV}}$	7.2 kV
Grid voltage (LV side)	V_{grid}	240 V
Line base impedance	Z_{line}	$V_{\text{grid}}^{\text{HV}^2}/S_t$
Line inductance	L_{line}	$0.05Z_{\text{line}}/\omega_o$ mH
Line resistance	R_{line}	$0.02Z_{\text{line}}$
Grid frequency	f_o	60 Hz
Switching frequency	f_{sw}	10 kHz

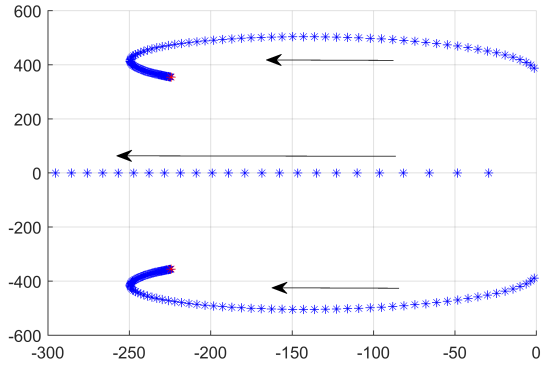

Fig. 5: Movement of dominant closed-loop poles of the 2-term PR current control approach when k varies.

The transfer function of L-filter G(s) as shown in Fig. 4 is described as, $G(s)=\frac{1}{sL+R}$.

A. 2-Term Proportional Resonant (PR) Controller

This is the most frequently used current controller approach for the grid-connected inverters, and it is generally referred simply as PR controller in the literature. The compensator $H_1(s)$ is described by $H_1(s) = \frac{kw_o s}{s^2+2\zeta\omega_o s+\omega_o^2}$. Reference [30] recommends that $\zeta \approx 0.001$, and guideline of [31] recommends that $H_2(s) = k$. The value of k is designed such that the pole in the real axis is not too far to cause the high-frequency issues and the dominant poles have sufficient damping.

Figure 5 shows the movement of closed loop poles for the parameters in Table I when k varies from 0 to 5. When $k = 5$, dominant poles are located at $[-209 \pm j340]$, and the non-dominant pole lying in real axis is at -3437.

It will be shortly shown that this conventional approach imposes a significant limitation on the control loop responses as the grid gets weaker.

B. 3-Term PR Controller

The existing current control approach in the previous section is improved by adding one extra control term in the numerator of $H_1(s)$ such that $H_1(s) = -\frac{k_{c2}s+k_{c1}\omega_o}{s^2+\omega_o^2}$ while $H_2(s) = k_p$ remains similar. These three gains $k = [k_p \;\; k_{\text{c1}} \;\; k_{\text{c2}}]$ are optimally designed to be used as a basis for subsequent comparisons with the proposed enhanced controller. Thus, state space representation of the current control loop (excluding the PLL branch) is given as

$$\begin{aligned} \dot{x}_p &= -\tfrac{R}{L}x_p + \tfrac{1}{L}u - \tfrac{1}{L}v_g \\ \dot{x}_{c1} &= \omega_o x_{c2}; \quad \dot{x}_{c2} = -x_p - \omega_o x_{c1} + i_{\text{ref}} \end{aligned} \tag{1}$$

where

$$X_{c1}(s) = \frac{\omega_o}{s^2+\omega_o^2}E(s), \;\; X_{c2}(s) = \frac{s}{s^2+\omega_o^2}E(s) \tag{2}$$

are the controller's state variables, $x_p \triangleq i_g$ is the plant variable (also the output), and $u = mV_{\text{dc}}$ is the control input, where m is the PWM modulating signal. Notice that the PWM gain is assumed to be unity, the inverter gain is V_{dc}, and therefore the total gain from before the division block to after the Inv block in Fig. 4 is unity. The control input is equal to

$$u = -k_p x_p - k_{c1}x_{c1} - k_{c2}x_{c2} \tag{3}$$

which is a full state feedback expression. The linear quadratic tracking (LQT) approach proposed in [32] and [33] is used to optimally design the controller gains as briefly described here. The control input u and the state vector x are transformed into v and z using the transformation $(\frac{d^2}{dt^2}+\omega_o^2)$. This implies $v = (\frac{d^2}{dt^2}+\omega_o^2)u$ and $z = (\frac{d^2}{dt^2}+\omega_o^2)x$. After transformation, equations (1) becomes

$$\dot{z}_p = -\frac{R}{L}z_p + \frac{1}{L}v, \;\; \dot{z}_{c1} = \omega_o z_{c2}, \;\; \dot{z}_{c2} = -z_p - \omega_o z_{c1} \tag{4}$$

which is represented in state space form as $\dot{z}(t) = Az + Bv$ where matrices A and B are

$$A = \begin{bmatrix} -\frac{R}{L} & 0 & 0 \\ 0 & 0 & \omega_o \\ -1 & -\omega_o & 0 \end{bmatrix}; B = \begin{bmatrix} \frac{1}{L} \\ 0 \\ 0 \end{bmatrix}. \tag{5}$$

In the above-mentioned derivation, it is assumed that the grid voltage and reference current are pure sinusoidal at frequency ω_o. Similarly, the control input is expressed as

$$v = -kz; \quad k = [k_p \;\; k_{c1} \;\; k_{c2}]. \tag{6}$$

It is evident from equation (2) that $z_{c1} = \omega_o e$ and $z_{c2} = \dot{e}$. In other words, the tracking error and its derivative are included among the new state variables. Guidelines given in [31] are followed to optimally design the controller gains to minimize the cost function

$$J = \int_0^\infty (q_1 z_p^2 + q_2\omega_o^2 e^2 + q_3\dot{e}^2 + v^2)dt \tag{7}$$

For the set of numbers defined in Table I, the optimal state feedback gains are obtained at $k = [2.5 \;\; 206.7 \;\; -1136.2]$, and the corresponding location for the closed-loop poles of the current controller is $[-1236 \;\; -348 \pm j227]$. The design stage involves sequentially increasing q_2, q_1 and q_3 and observing their impact on the closed loop poles. In Fig. 6, q_2 is increased from 10^1 to $10^{4.84}$, then q_1 is increased from 10^{-2} to $10^{0.5}$ and finally q_3 is increased from 10^1 to $10^{6.1}$. Current controllers designed using this optimal control approach have very high robust performance as compared with existing non-optimal designs [31], [32], [34]. The weak grid conditions, however,

This article has been accepted for publication in a future issue of this journal, but has not been fully edited. Content may change prior to final publication. Citation information: DOI 10.1109/TPEL.2019.2909532, IEEE Transactions on Power Electronics

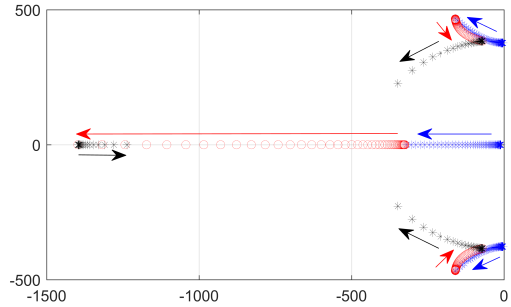

Fig. 6: Movement of closed-loop poles (of existing current control approach) when q_2(blue), q_1(red) and q_3(black) vary.

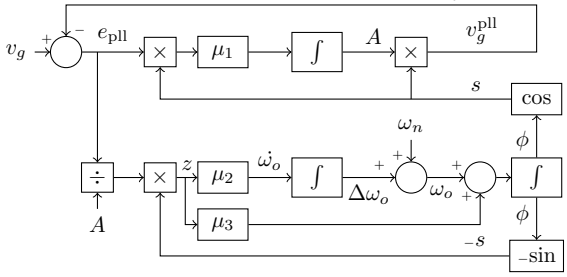

Fig. 7: EPLL

are not specifically formulated in the existing or optimal design methods. The following section proposes an optimal control theory based design formulation for this problem.

C. Proposed Controller

This section introduces a new approach to restructuring and designing the inverter current controller to enhance its transient responses, especially in weak grid conditions. The proposed approach is based on 1) including the grid impedance in the design, and 2) including the PLL state variables among the entire system state variables and use them to generate the control input. The grid voltage is no longer treated as a stiff voltage in the proposed method. The proposed structure is shown in Fig. 4. The PLL variables are used in the feedback loop through the two new gains $[k_{1\text{pll}} \;\; k_{2\text{pll}}]$. The PLL used in the proposed controller is the EPLL shown in Fig. 7 [35].

1) System Modeling and State Equations: **Plant:** Use the same definition of $x_p = i_g$ and $u = v_{\text{inv}} = mV_{\text{dc}}$. The grid impedance can be included in the model along with the filter inductance using the Kirchhoff's voltage law. The grid voltage at PCC of the inverter is denoted by v_g and the remote (and unavailable) grid voltage is denoted by v_{grid}. Feed-forward of the grid voltage supplied by the PLL, i.e. v_g^{pll}, is normally ignored in existing system modeling approaches. In our study, this signal is included among the EPLL state variables as $x_{2\text{pll}}$, as seen in the following paragraph, and is included in the modeling. Therefore, the extended equation of the inverter current may be derived as

$$\dot{x}_p = -\frac{R+R_g}{L+L_g}x_p + \frac{1}{L+L_g}x_{2\text{pll}} + \frac{1}{L+L_g}u - \frac{1}{L+L_g}v_{\text{grid}}. \quad (8)$$

Resonant Controller: State equations of the PR controller remain the same as in conventional controller. These are the second and third equations in (1).

PLL: An LTI model for the EPLL can be derived ignoring the dynamics of $\Delta\omega_o$ and by properly defining its state variables. Let A and ϕ be the peak value and phase of input v_g as determined by EPLL. Considering $\mu_1 = \mu_3 = \mu$ in Fig. 7, dynamics of the EPLL is represented by

$$\dot{A} = \mu e_{\text{pll}} \cos(\phi), \quad \dot{\phi} = \omega_o - \frac{\mu e_{\text{pll}}}{A}\sin(\phi). \quad (9)$$

Define two EPLL state variables as $x_{1\text{pll}} = \frac{A}{\omega_o}\sin(\phi)$ and $x_{2\text{pll}} = v_g^{\text{pll}} = A\cos(\phi)$. Differentiating these two and substituting from (9) leads to

$$\dot{x}_{1\text{pll}} = x_{2\text{pll}}, \quad \dot{x}_{2\text{pll}} = \mu e_{\text{pll}} - \omega_o^2 x_{1\text{pll}} \quad (10)$$

where $e_{\text{pll}} = v_g - v_g^{\text{pll}} = v_g - A\cos(\phi) = v_g - x_{2\text{pll}}$. Since v_g is not a stiff voltage, its dynamics in terms of other variables and the stiff voltage v_{grid} can easily be derived as

$$v_g = \alpha_1 x_p + \alpha_3 x_{2\text{pll}} + \alpha_3 u + \alpha_2 v_{\text{grid}} \quad (11)$$

where $\alpha_1 = \frac{LR_g - L_g R}{L+L_g}$, $\alpha_2 = \frac{L}{L+L_g}$, and $\alpha_3 = \frac{L_g}{L+L_g}$.

Substituting v_g in e_{pll} and e_{pll} in $\dot{x}_{2\text{pll}}$, the second EPLL equation is expressed as

$$\dot{x}_{2\text{pll}} = \mu\alpha_1 x_p - \omega_o^2 x_{1\text{pll}} - \mu\alpha_2 x_{2\text{pll}} + \mu\alpha_3 u - \mu\alpha_2 v_{\text{grid}}. \quad (12)$$

The total system state variables are x_p, x_{c1}, x_{c2}, $x_{1\text{pll}}$ and $x_{2\text{pll}}$. Their dynamics are derived and expressed above. With this definition of state variables, the control input is equal to

$$u = -k_p x_p - k_{c1}x_{c1} - k_{c2}x_{c2} - k_{1\text{pll}}x_{1\text{pll}} - k_{2\text{pll}}x_{2\text{pll}} \quad (13)$$

which is in the form of a full state feedback. The optimal design of this five gains is discussed in the following section.

2) Optimal Design of Proposed Controller: In order to use the LQT formulation of [32], [33], the state equations are linearly transformed by applying $(\frac{d^2}{dt^2} + \omega_o^2)$. With definitions of $z = (\frac{d^2}{dt^2} + \omega_o^2)x$ and $v = (\frac{d^2}{dt^2} + \omega_o^2)u$, state equations and control law are re-written as

$$\begin{aligned}
\dot{z}_p &= -\frac{R+R_g}{L+L_g}z_p - \frac{1}{L+L_g}z_{2\text{pll}} + \frac{1}{L+L_g}v \\
\dot{z}_{c1} &= \omega_o z_{c2}; \quad \dot{z}_{c2} = -z_p - \omega_o z_{c1} \\
\dot{z}_{1\text{pll}} &= z_{2\text{pll}} \\
\dot{z}_{2\text{pll}} &= \mu\alpha_1 z_p - \omega_o^2 z_{1pll} - \mu\alpha_2 z_{2\text{pll}} + \mu\alpha_3 v \\
v &= -kz; \quad k = [k_p \;\; k_{c1} \;\; k_{c2} \;\; k_{1\text{pll}} \;\; k_{2\text{pll}}].
\end{aligned} \quad (14)$$

These equations in (14) are expressed in state space form as $\dot{z} = A_p z + B_p v$ where the matrices A_p and B_p are given by

$$A_p = \begin{bmatrix} -\frac{R+R_g}{L+L_g} & 0 & 0 & 0 & \frac{1}{L+L_g} \\ 0 & 0 & \omega_o & 0 & 0 \\ -1 & -\omega_o & 0 & 0 & 0 \\ 0 & 0 & 0 & 0 & 1 \\ \mu\alpha_1 & 0 & 0 & -\omega_o^2 & -\mu\alpha_2 \end{bmatrix}, B_p = \begin{bmatrix} \frac{1}{L+L_g} \\ 0 \\ 0 \\ 0 \\ \alpha_3\mu \end{bmatrix}.$$

This approach will transform the state variables such that $z_{c1} = \omega_o e$ and $z_{c2} = \dot{e}$. The cost function $J = \int_0^\infty (z^T Q_p z + v^2)dt$ will then directly engage the tracking error and its derivative. It can be minimized for finding the controller gains using the popular LQR technique. The positive semi-definite matrix Q_p is diagonal with entries q_i, $i = 1, 2, 3, 4, 5$. The full design stage is described below.

Selection of μ:

The input-output relationship for LTI-EPLL described by equation (9) can be described by the transfer function

$$\frac{Y_{\text{pll}}(s)}{U_{\text{pll}}(s)} = \frac{\mu s}{s^2 + \mu s + \omega_o^2}. \quad (15)$$

If $\mu \triangleq 2\zeta_1\omega_o$ is defined, ζ_1 corresponds to the damping of poles of LTI-EPLL. It is recommended to select μ corresponding to $\zeta_1 \in [0.7, 0.9]$ so that these poles are well

This article has been accepted for publication in a future issue of this journal, but has not been fully edited. Content may change prior to final publication. Citation information: DOI 10.1109/TPEL.2019.2909532, IEEE Transactions on Power Electronics

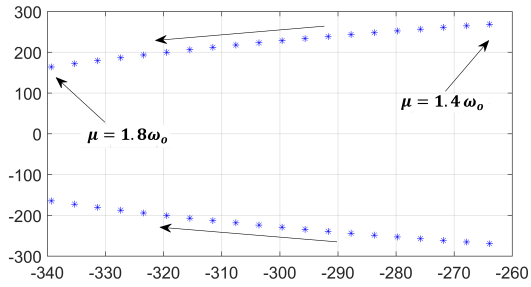

Fig. 8: Movement of EPLL poles for $\mu \in [1.4\omega_o, 1.8\omega_o]$

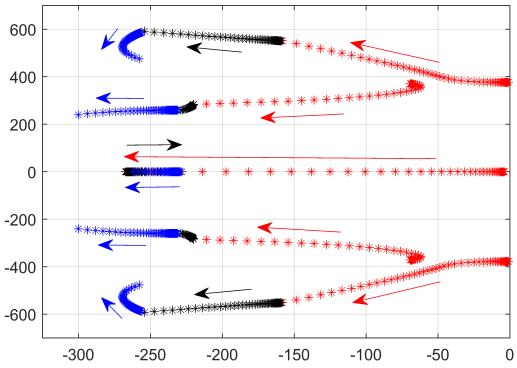

Fig. 9: Movement of all poles when q_2(red), q_3(black), and q_5(blue) change.

placed initially. Figure 8 shows the movement of linear EPLL poles for $\mu \in [1.4\omega_o, 1.8\omega_o]$. These poles are subject to change subsequently during the selection of Q_p, however, initializing them in the range as shown in Fig. 8 enables to suitably and conveniently place all closed loop system poles. The parameter μ_2 in Fig. 7 is selected according to $\mu_2 = \frac{\mu^2}{8\zeta_2^2}$ where ζ_2 is a damping factor [29].

Selection of Q_p:

Initialize q_1 to q_5 at small non-negative numbers.

Step I: Start with q_2 and increase it until the tracking error builds up to a desirable shape. This term increases the weight of the tracking error in the cost function. Freeze q_2.

Step II: Increase the value of q_3 gradually until the dominant poles have desirable speed. Notice that this term increases the weight of the derivative of the tracking error in the cost function. Freeze q_3 too.

Step III: Increase the value of q_5 gradually until all five poles have the desired speed and damping. Notice that this term increases the weight of the PLL feedback terms in the cost function.

Figure 9 shows the evolution of all closed-loop poles. The value of $\mu = 1.5\omega_o$ is selected so that $\zeta_1 = 0.75$ is within the recommended range. In Fig. 9, movement of poles is shown for q_2 varying from 10^0 to $10^6.1$ (red asterisks), q_3 varying from 10^0 to $10^6.2$ (black asterisks), and q_5 varying from 10^{-1} to $10^{0.2}$. This gives the value of designed controller gains as $k = [4.2\ 463.0\ -1621.5\ -8.6\ 1.0]$ and poles are located at $[-262, -300 \pm j240, -258 \pm j476]$.

IV. Inverter Current Controller with LCL Filter

Assume that the output filter of the inverter is in the form of an LCL where L_1, C_1, and L_2 are the inverter side inductor, parallel capacitor and the grid side inductor, respectively. Similarly, let R_d be the damping resistance in series with C_1 and, R_1 and R_2 be corresponding resistances of inductors L_1 and L_2. Let, i_1 be current through L_1, v_c be voltage across C_1, and i_2 be current through L_2 or inverter output current.

Considering the resonant frequency of LCL filter $f_r = \frac{f_{sw}}{4}$ and attenuation of switching noises to be 6 times that of L-filter, [$L_1 = 0.33$ mH, $L_2 = 0.20$ mH, $C_1 = 8.2\ \mu F$] is chosen for the system described in section II. The controller gains are designed such that the dominant poles have desired damping and response time.

A. 2-Term PR Controller

Two-term PR controller approach can be applied only for the passive damping in the LCL filter. The minimum possible damping resistance R_d is chosen without compromising the high-frequency stability of the system.

Similar to the L-filter, the compensator $H_1(s)$ and filter transfer function $G(s)$ for this approach are described by

$$H_1(s) = \frac{kw_o s}{s^2 + 2\zeta\omega_o s + \omega_o^2}$$
$$G(s) = \frac{C_1 R_d s + 1}{L_1 C_1 L_2 s^3 + (L_1 + L_2) C_1 R_d s^2 + (L_1 + L_2) s} \quad (16)$$

and following the guideline of [31], $H_2(s) = k$ is chosen. The value of k is designed having a trade-off between high-frequency and low-frequency stability of the systems. The design guideline is as follows.

Step I: Choose a value of R_d such that power loss is less than 0.5% of inverter rating.

Step II: Gradually increase the value of k such that low-frequency poles have sufficient damping.

Step III: Check the high-frequency poles of LCL filter. If they are not well damped, slightly increase R_d and repeat from Step-I.

Figure 10 shows the movement of closed-loop dominant poles for $R_d = 0.75\ \Omega$ and k varying from 0.01 to 2.0. The value of $k = 2.0$ is chosen for which high-frequency poles are at $[-1146 \pm j31602]$ with damping close to 0.035 and low-frequency dominant poles are at $[-210 \pm j340]$ with damping of 0.53. One non-dominant pole in the real axis is at -3347. This controller design has excellent performance for normal grid conditions, but it degrades as the grid becomes weaker.

B. Proposed controller

The compensators $H_1(s)$ and $H_2(s)$ in Fig. 4 are described by the same transfer functions as for L-filter in section III-B. Active damping is adopted for this approach, i.e.$R_d = 0\ \Omega$ and thus the filter transfer function $G(s)$ becomes is

$$G(s) = \frac{1}{L_1 C_1 L_2 s^3 + (L_1 + L_2) s}. \quad (17)$$

The controller gains are optimally designed including grid and EPLL dynamics as in proposed controller for L-filter. The three state variables for LCL filter are naturally defined as $x_{p1} = i_1$, $x_{p2} = v_c$, and $x_{p3} = i_2$. Along with resonant

This article has been accepted for publication in a future issue of this journal, but has not been fully edited. Content may change prior to final publication. Citation information: DOI 10.1109/TPEL.2019.2909532, IEEE Transactions on Power Electronics

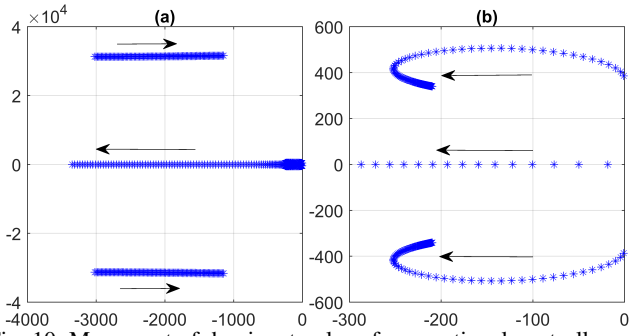

Fig. 10: Movement of dominant poles of conventional controller with LCL filter when k change. (a) All pole locations where non-dominant poles are visible. (b) Dominant poles.

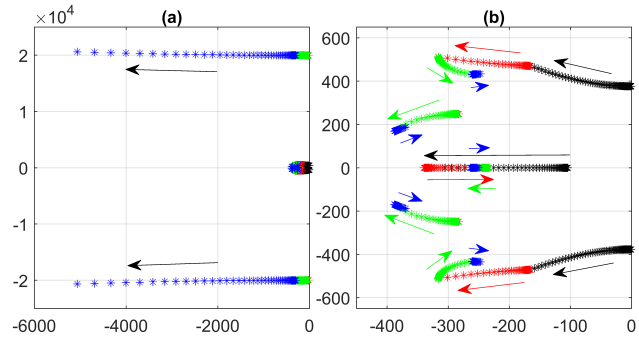

Fig. 11: Movement of dominant poles for proposed controller with LCL filter when q_4 (black), q_5 (red), q_7 (green), and q_2 (blue) change.(a) All pole locations where non-dominant poles are visible. (b) Dominant poles.

controller and EPLL equations from (1) and (9), overall system including grid impedance is described by following equations.

$$\begin{aligned}
\dot{x}_{\rm p1} &= -\frac{R_1}{L_1}x_{\rm p1} - \frac{1}{L_1}x_{\rm p2} + \frac{1}{L_1}u \\
\dot{x}_{\rm p2} &= \frac{1}{C_1}x_{\rm p1} - \frac{1}{C_1}x_{\rm p3} \\
\dot{x}_{\rm p3} &= \frac{1}{L_2+L_g}x_{\rm p2} - \frac{R_2+R_g}{L_2+L_g}x_{\rm p3} - \frac{1}{L_2+L_g}v_{grid} \\
\dot{x}_{\rm c1} &= \omega_o x_{\rm c2}; \quad \dot{x}_{\rm c2} = -x_{\rm p3} - \omega_o x_{\rm c1} + i_{\rm ref} \\
\dot{x}_{\rm 1pll} &= x_{\rm 2pll} \\
\dot{x}_{\rm 2pll} &= \mu\beta_3 x_{\rm p2} + \mu\beta_1 x_{\rm p3} - \omega_o^2 x_{\rm 1pll} - \mu x_{\rm 2pll} - \mu\beta_2 v_{\rm grid}
\end{aligned} \tag{18}$$

where $\beta_1 = \frac{L_2R_g - L_gR_2}{L_2+L_g}$, $\beta_2 = \frac{L_2}{L_2+L_g}$, and $\beta_3 = \frac{L_g}{L_2+L_g}$. The control input is equal to

$$\begin{aligned}
u = &- k_{\rm p1}x_{\rm p1} - k_{\rm p2}x_{\rm p2} - k_{\rm p3}x_{\rm p3} - k_{c1}x_{c1} \\
&- k_{c2}x_{c2} - k_{\rm 1pll}x_{\rm 1pll} - k_{\rm 2pll}x_{\rm 2pll}.
\end{aligned} \tag{19}$$

The linear quadratic tracking (LQT) approach of [32], [33] is used to optimally design the control gains. Thus, the input (u) and the state (x) are transformed into v and z domain with transformations $v = (\frac{d^2}{dt^2} + \omega_o^2)u$ and $z = (\frac{d^2}{dt^2} + w_o^2)x$. System equations after transformations are written as

$$\begin{aligned}
\dot{z}_{\rm p1} &= -\frac{R_1}{L_1}z_{\rm p1} - \frac{1}{L_1}z_{\rm p2} + \frac{1}{L_1}v \\
\dot{z}_{\rm p2} &= \frac{1}{C_1}z_{\rm p1} - \frac{1}{C_1}z_{\rm p3} \\
\dot{z}_{\rm p3} &= \frac{1}{L_2+L_g}z_{\rm p2} - \frac{R_2+R_g}{L_2+L_g}z_{\rm p3} \\
\dot{z}_{\rm c1} &= \omega_o z_{\rm c2}; \quad \dot{z}_{\rm c2} = -z_{\rm p3} - \omega_o z_{\rm c1} \\
\dot{z}_{\rm 1pll} &= z_{\rm 2pll}; \\
\dot{z}_{\rm 2pll} &= \mu\beta_3 z_{\rm p2} + \mu\beta_1 z_{\rm p3} - \omega_o^2 z_{\rm 1pll} - \mu z_{\rm 2pll}
\end{aligned} \tag{20}$$

which is represented in state space form as $\dot{z} = Az + Bv$ where matrices A and B are

$$A = \begin{bmatrix}
-\frac{R_1}{L_1} & -\frac{1}{L_1} & 0 & 0 & 0 & 0 & 0 \\
\frac{1}{C_1} & 0 & -\frac{1}{C_1} & 0 & 0 & 0 & 0 \\
0 & \frac{1}{L+L_g} & -\frac{R_2+R_g}{L_2+L_g} & 0 & 0 & 0 & 0 \\
0 & 0 & 0 & 0 & \omega_o & 0 & 0 \\
0 & 0 & -1 & -\omega_o & 0 & 0 & 0 \\
0 & 0 & 0 & 0 & 0 & 0 & 1 \\
0 & \mu\beta_3 & 0 & \mu\beta_1 & 0 & -\omega_o^2 & -\mu
\end{bmatrix},$$

$$B = \begin{bmatrix} \frac{1}{L_1} & 0 & 0 & 0 & 0 & 0 & 0 \end{bmatrix}^T.$$

Similarly, the control input is expressed as

$$v = -kz; \quad k = [k_{\rm p1}\ k_{\rm p2}\ k_{\rm p3}\ k_{c1}\ k_{c2}\ k_{\rm 1pll}\ k_{\rm 2pll}]. \tag{21}$$

Similar to earlier section with L-filter, cost function $J = \int_0^\infty (z^T Q_p z + v^2)dt$ is minimized for finding the controller gains using the popular LQR technique. Note that $z_{\rm c1} = \omega_o e$ and $z_{\rm c2} = \dot{e}$. The positive semi-definite matrix Q_p is diagonal with entries q_i, $i = 1, 2, .., 7$ which is selected following the steps given below.

Step I: Start with q_4 and increase it until the tracking error builds up to a desirable shape.

Step II: Increase the value of q_5 gradually until the dominant poles have desirable speed.

Step III: Increase the value of q_7 to get enough feedback of EPLL states variables.

Step IV: Increase the value of q_2 to get desired damping of complex dominant poles.

Step V: The value of other q_i's are kept close to zero as they have little or no impact in pole placement.

Figure 11 shows the movement of closed-loop dominant poles for q_4 varying from 10^0 to 10^6 (black asterisks), q_5 varying from 10^0 to $10^{6.3}$ (red asterisks), q_7 varying from 10^{-2} to $10^{0.1}$(green asterisks), and q_2 varying from 10^{-4} to $10^{-0.5}$(blue asterisks). This gives the value of designed controller gains as $k = [3.5\ 0.16\ 0.21\ 617.18\ -1616.66\ 24.17\ 0.18]$ and poles are located at $[-250,\ -248 \pm 434i,\ -369 \pm 188i]$. Two non-dominant poles are at $[-5061 \pm 20619i]$.

C. Robustness of proposed controller to weak grid

Robustness of the proposed and conventional controllers are compared in this section using an eigenvalue analysis when the grid inductance L_g is uncertain. As shown in Fig. 12, the poles of conventional controller experience much larger level of change compared to the poles of the proposed controller. This confirms higher level of robustness of the proposed controller.

V. Simulation Results

Simulations are performed in PSIM software for parameters in Table I and designed controller gains. The rating of the grid as described in the appendix is kept fixed at 50 kVA and grid impedance is gradually increased to weaken the grid. Grid voltage and frequency experience oscillations subsequent to any disturbance causing a temporary imbalance in the load and generation.

This article has been accepted for publication in a future issue of this journal, but has not been fully edited. Content may change prior to final publication. Citation information: DOI 10.1109/TPEL.2019.2909532, IEEE Transactions on Power Electronics

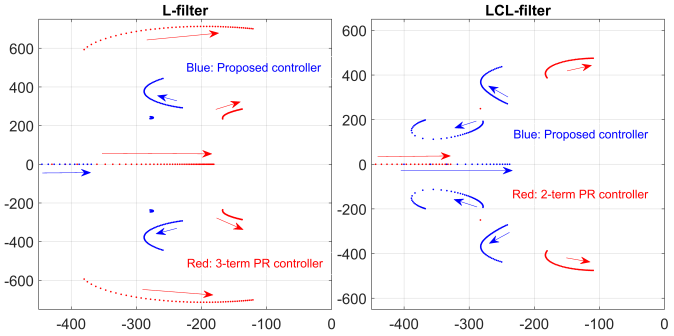

Fig. 12: Eigenvalues of the proposed and conventional controllers when L_g varies from 1 mH to 4 mH.

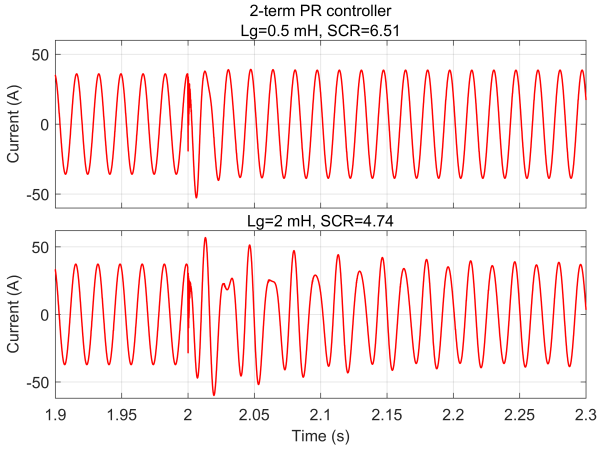

Fig. 13: Response of 2-Term PR controller with L-filter when local load is disconnected at $t = 2$ s.

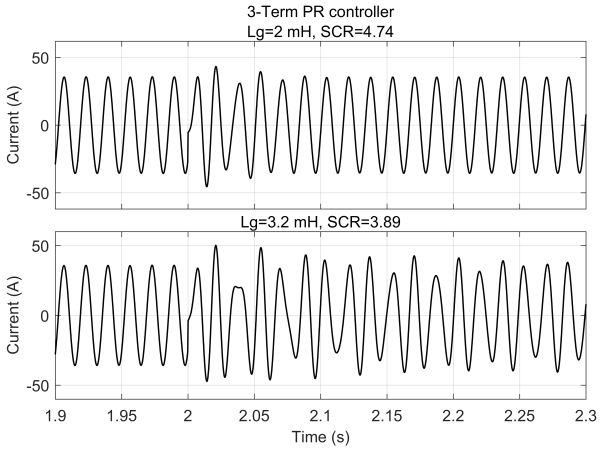

Fig. 14: Responses of 3-Term PR controller with L-filter when local load is disconnected at $t = 2$ s.

The operation and grid-connection of the inverter are done sequentially. At first, the PLL is started and v_g^{pll} is feed-forwarded. Then, the current controller is started so that control input (u) is generated. Control input is used to generate switching pulses for power electronic switches and applied to them.

Initially, the inverter is operating at the rated condition with a local load connected. At time $t = 2$ s, the local load is disconnected to observe its effect on overall current, voltage and frequency of the system.

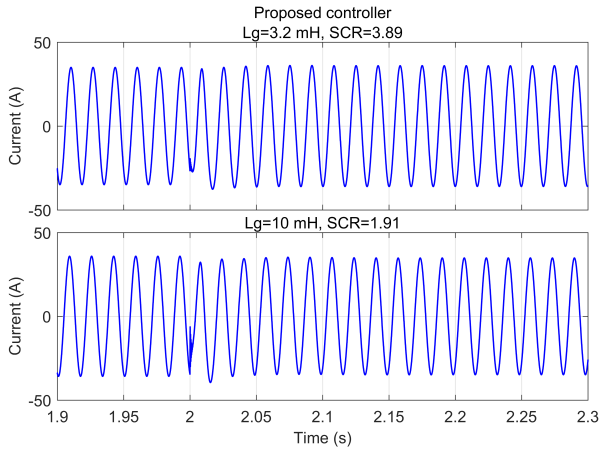

Fig. 15: Responses of proposed controller with L-filter when local load is disconnected at $t = 2$ s.

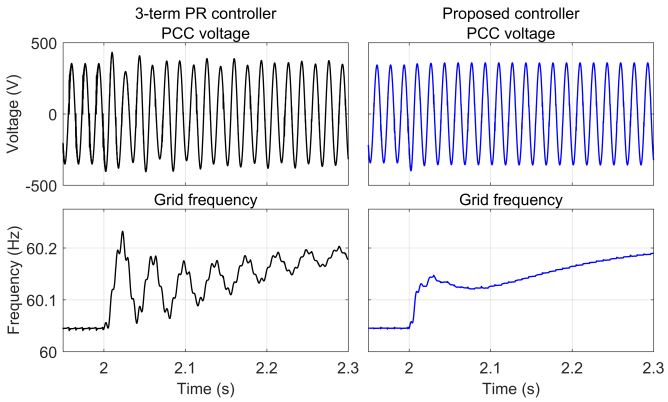

Fig. 16: PCC voltage and PLL frequency of proposed and 3-term PR controller with L-filter when local load is disconnected at $t = 2$ s.

A. Simulation Results with L-Filter

Figure 13 shows the performance of 2-term PR controller with L-filter. When the grid inductance is $L_g = 0.5$ mH, the grid is strong with high SCR and thus the inverter output current has little oscillations when the local load is disconnected. However, when grid inductance L_g is increased barely to 2 mH, the inverter output current as shown in Fig. 13 is oscillatory and is on the verge of instability. For the same value of grid impedance, the 3-term PR controller still has acceptable performance with oscillations only for few cycles as shown in Fig. 14. This 3-term PR controller slightly improves the robustness of the system reaching its instability limit for the grid inductance of $L_g = 3.2$ mH.

The performance of the proposed controller is depicted in Fig. 15. It has an excellent performance not only for the cases when both 2-term and 3-term PR controller become unstable, but also when the grid is extremely weak. The inverter output current as shown in Fig. 15 has almost no oscillations even for $L_g = 10$ mH when local load is disconnected. Therefore, the proposed current controller has a robust performance for all practical weak grid conditions. It is worthwhile mentioning that, although this study is done for a given inverter power rating, similar conclusions about these controller design approaches can be drawn for all practical inverter ratings.

Furthermore, Fig. 16 compares transients of PCC voltage and its frequency as measured by the EPLL during local load change for grid inductance of $L_g = 3.2$ mH. The response of

This article has been accepted for publication in a future issue of this journal, but has not been fully edited. Content may change prior to final publication. Citation information: DOI 10.1109/TPEL.2019.2909532, IEEE Transactions on Power Electronics

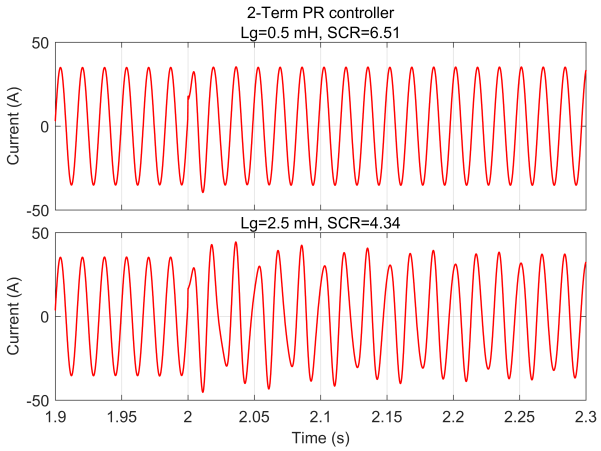

Fig. 17: Responses of 2-term PR controller with LCL-filter when local load is disconnected at $t = 2$ s.

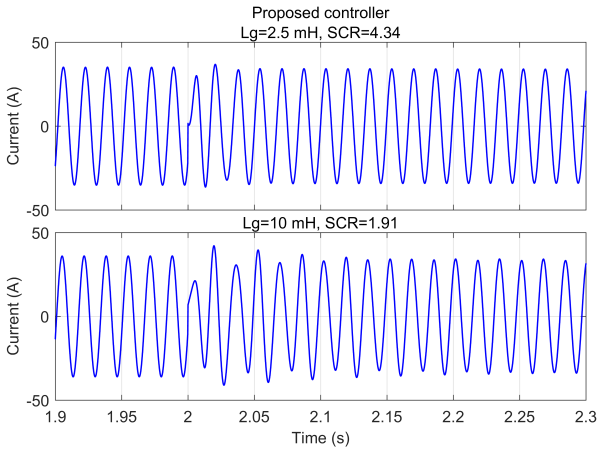

Fig. 18: Responses of proposed controller with LCL-filter when local load is disconnected at $t = 2$ s.

3-Term PR controller has much oscillations in both the voltage magnitude and frequency while that of the proposed controller has much lower oscillations. These oscillations are reflected in the inverter output currents shown in Fig. 14 and Fig. 15.

B. Simulation Results with LCL Filter

The performances of different controllers with LCL filter are similar to that with L filter. Figure 17 shows that the performance of 2-term PR controller with LCL filter is excellent during strong grid condition i.e. when $L_g = 0.5$ mH, and it reaches on the brink of instability for a relatively weaker grid when $L_g = 2.5$ mH. In contrast, the proposed controller has excellent performance for $L_g = 2.5$ mH and acceptable performance for extremely weak grid condition with $L_g = 10$ mH as shown in Fig. 18. As expected, current controllers for the LCL filter are found to be more sensitive to the grid disturbances such as local load changes as compared to the controller for the L filter.

VI. Experimental Results

The experimental set-up is shown in Fig. 19. A SEMISTACK-IGBT module is used to implement the inverter. The conventional and proposed control systems are implemented on a TMSF28335 DSP by programming in Code Composer Studio V6.2. A Chroma 63800 programmable load and a Sorensen XG 600-1.4 programmable dc power supply are used to model a load and dc source respectively. An MI 2883 EU Class S power quality analyzer is used for monitoring the power quality. All circuit parameters are listed in Table II. The inverter and local load are connected to the actual grid. Since the grid is very stiff, a relatively large inductance (L_g) is inserted to weaken the grid such that some oscillations can be observed. The used inductors are not of high quality and they caused additional harmonics to the voltage at the point of connection. Three different tests are performed as described below.

TABLE II: Circuit parameters of experimental test set-up

L-filter inductance	L	1.4 mH
DC-bus voltage	V_{dc}	200 V
Grid inductance	L_g	4.5 mH
Grid frequency	f_o	50 Hz
Grid voltage	v_s	110 V
Switching frequency	f_{sw}	10 kHz

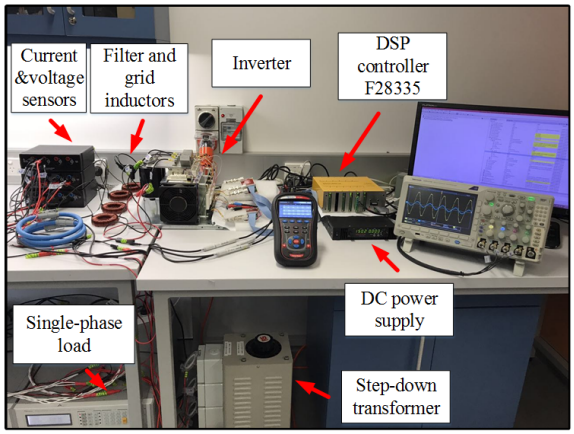

Fig. 19: Experimental test set-up.

Test I (Start-up): Figure 20 shows the start-up of inverter for conventional and proposed controllers. The grid voltage (yellow trace), the inverter current (blue trace) and the grid voltage peak magnitude estimated by the PLL (green trace) are shown. The inverter starts injecting 3.2 A (350 W) into the grid. The proposed controller start-up is smoother than the conventional controller with much small transients and oscillations. Figure 21 compares the harmonic spectrum of the three controllers for this operating condition—which are the conventional controller, as well as the proposed controller with and without the EPLL error (e_{pll} passed through a low-pass filter with the cut-off frequency of 1 kHz and added as shown in Fig. 4. These results are generated by an MI 2883 EU Class S power quality analyzer. The THD of the inverter's output current using the conventional method is 16%, using the proposed method without EPLL feedback is 8% and after connecting the EPLL error is 4.7%.

Test II (Inverter Current Reduction): In this test, the dynamic of the system is tested in a weak grid when the inverter output current reduces from 4.2 A (460 W) to 0 A (0 W) abruptly. As shown in Fig. 22 (a), this causes an oscillation on the grid voltage when the system is controlled by the

This article has been accepted for publication in a future issue of this journal, but has not been fully edited. Content may change prior to final publication. Citation information: DOI 10.1109/TPEL.2019.2909532, IEEE Transactions on Power Electronics

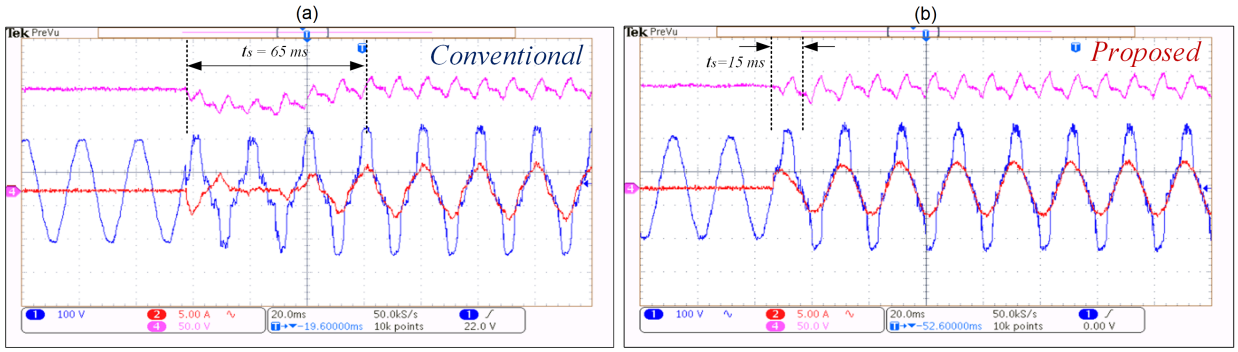

Fig. 20: Start-up transients for controllers (Test I).

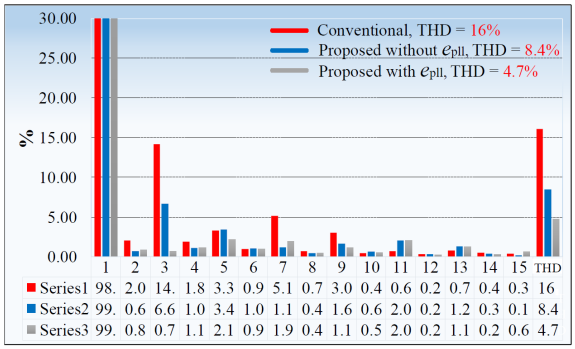

Fig. 21: THD of inverter output current.

conventional controller, whereas the response of the proposed controller, shown in Fig. 22 (b), are robust with a much lower interaction between the grid and inverter. Notice that the large 4.5 mH inductor used to weaken the grid for experimental testing amplifies the harmonics of the grid-voltage during the operation of the converter.

Test III (Local Load Disconnection): The local load of 700 W is disconnected while the inverter is injecting 50 W into the grid. As shown in Fig. 23 (a), this causes an oscillation in the grid voltage and also the inverter current when the conventional controller is used. The proposed controller, on the other hand, rides through this smoothly with much smaller impacts as shown in Fig. 23 (b).

VII. Performance of Proposed Controller in Distorted Grid Conditions

This section presents power quality aspects of the proposed controller. Particularly, its performance when the grid voltage is distorted is studied in detail. It is observed that the proposed controller, in addition to significantly enhancing the weak grid performance, also enhances the power quality aspects of the inverter. An additional innovative term is included in the controller to further improve the power quality aspects.

Figure 24 shows the magnitude Bode plot of $\frac{I_g(s)}{V_g(s)}$ for both conventional and proposed controller for different inverter power ratings. It also shows corresponding percentage total harmonic distortion (THD) of the inverter current versus to percentage THD of the grid voltage.

The fundamental component of I_g increases in the same proportion with the inverter power rating for the same value of nominal grid voltage. As seen in Fig. 24 (top-left panel), harmonic attenuation level gradually decreases as the inverter power rating increases for the conventional controller. As a result, the THD of I_g in the conventional controller decreases while inverter power rating increases from 2 kW to 5 kW, but it does not decrease further because the attenuation of harmonics decreases for higher power rating as seen in Fig. 24 (top-right panel). In contrast, the attenuation level is more robust and remains fairly constant for the proposed controller, Fig. 24 (bottom-left panel). As a result, in the proposed controller, the THD of I_g constantly decreases with an increase in the inverter power rating as expected and is verified in Fig. 24 (bottom-right panel).

The harmonic rejection capability of the proposed controller is further enhanced by introducing the EPLL error as a feed-forward in the controller. The error signal e_{pll} of the EPLL as seen in Fig. 7 is added to v_g^{pll} after filtering through a low pass filter (F) of suitable cutoff frequency (f_c) as show in Fig. 4. This feed-forward of error can contribute to mitigating the harmonics introduced by the grid voltage. This is supported by the mathematical analysis employing the magnitude Bode plot as shown in Fig. 25. The additional dip in the bode plot in the frequency region of $10^2 - 10^3$ Hz is created by this scheme and it shows that the dominant lower harmonics are attenuated. This is verified through simulations and shows a significant drop in the THD of inverter current for inverter power ratings of 2-10 kW in Fig. 25 as compared to that of Fig. 24.

Introducing EPLL error in feed-forward significantly improves the harmonic rejection ability of the proposed controller. However, we should be careful in selecting filter cut off frequency (f_c). Higher f_c would allow a higher range of harmonics to pass through the filter and reduce THD in I_g, but at the same time, it makes control system more susceptible to high-frequency noises and disturbances. Figure 26 shows that THD in I_g significantly drops as f_c increases up to about 1 kHz for all power ratings of inverter. After that, it saturates and does not contribute effectively. Therefore, it is recommended to select f_c around one kHz so as to minimize the THD without introducing high-frequency noise and dynamics of v_g into the control system. Figure 27 shows inverter output current for two different inverter power ratings when THD in v_g is 6.0%. The THD of grid current is found to be 10.28% and 5.90% for the conventional controller of inverter ratings of 2 kW and 10 kW, respectively. For the proposed controller, the THD of the grid current is reduced to 6.24% and 2.14% for inverter ratings of 2 kW and 10

This article has been accepted for publication in a future issue of this journal, but has not been fully edited. Content may change prior to final publication. Citation information: DOI 10.1109/TPEL.2019.2909532, IEEE Transactions on Power Electronics

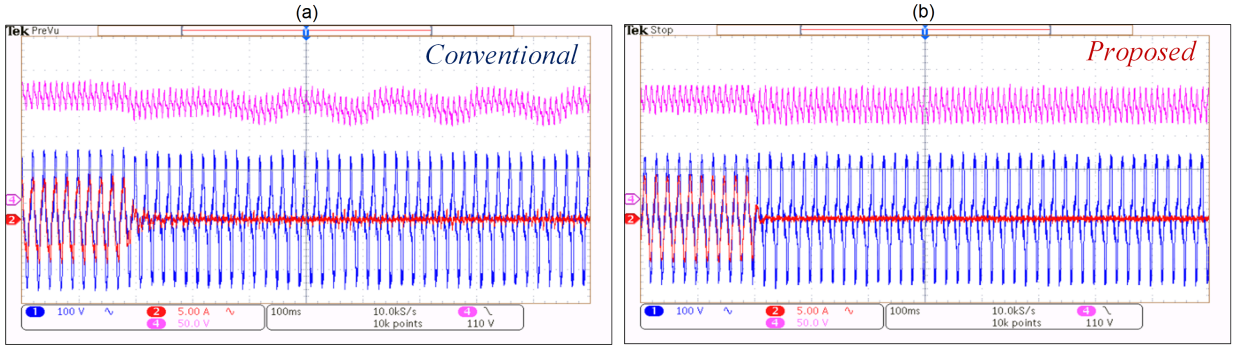

Fig. 22: Response of controllers during weak grid condition when inverter output is suddenly reduced (Test II).

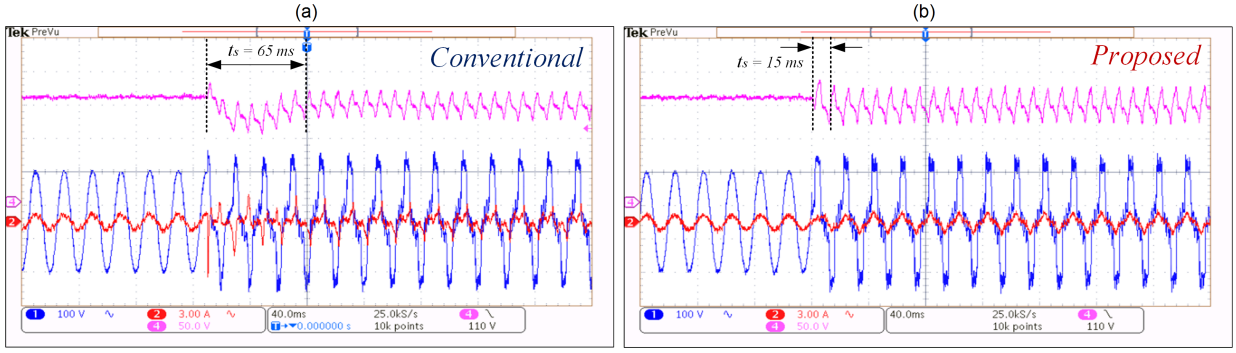

Fig. 23: Response of controllers when local load is disconnected (Test III).

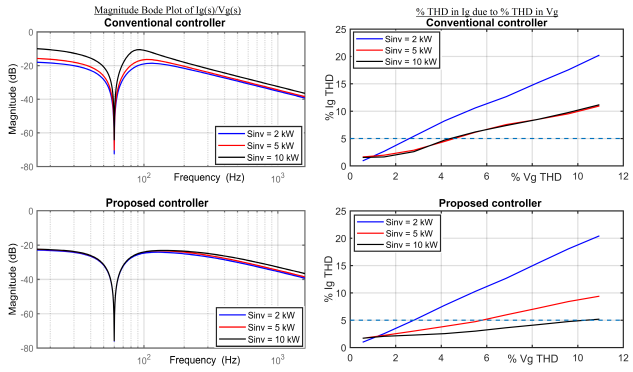

Fig. 24: Magnitude Bode plots of conventional and proposed controllers for different inverter power ratings (left). Inverter current THD versus grid voltage THD for different inverter power ratings (right).

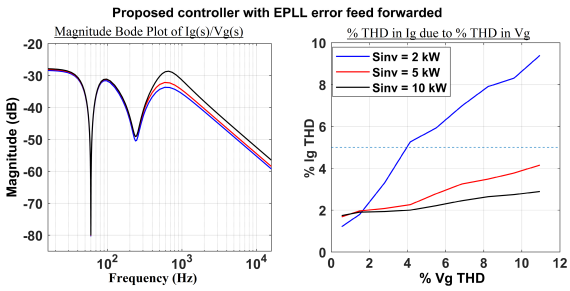

Fig. 25: Magnitude Bode plot of proposed controller with the EPLL error feed forwarded for different power ratings (left panel). Inverter current THD versus grid voltage THD of the proposed system for different power ratings (right panel).

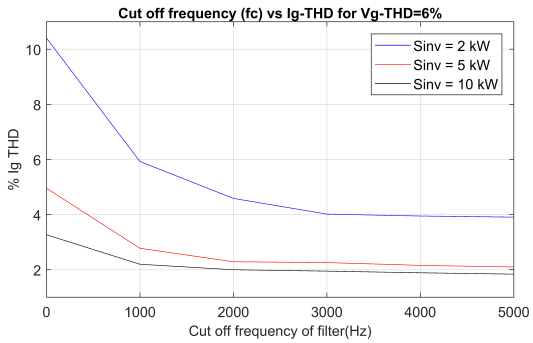

Fig. 26: Effect of filter cutoff frequency (f_c) on THD of I_g for different power ratings

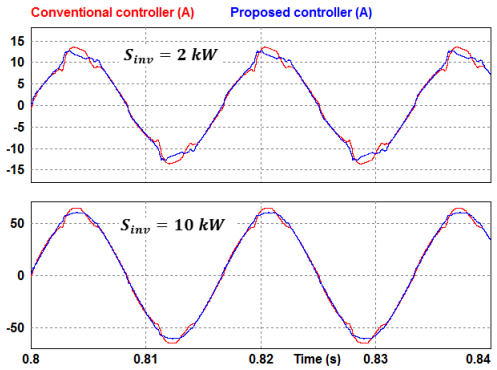

Fig. 27: Inverter output current for both controllers when THD in v_g is 6.0%

kW, respectively. This improvement is visible in the current waveform shown in Fig. 27. The presented THD analysis concerns harmonics within reasonable range, e.g. up to 30th harmonic which is 1800 Hz. If the switching frequency is decreased to 2 kHz, and the interfacing inductance is adjusted accordingly, the presented THD analysis results will still be valid. For switching frequencies below 2 kHz, the switching harmonics will interfere with those harmonics.

This article has been accepted for publication in a future issue of this journal, but has not been fully edited. Content may change prior to final publication. Citation information: DOI 10.1109/TPEL.2019.2909532, IEEE Transactions on Power Electronics

TABLE III: Parameters of synchronous machine

Parameters	Symbol	Value
Generator/Grid rating	S	50 kVA
Rated phase voltage	V_{gH}	7.2 kV
Number of poles	n_p	2
Moment of inertia	J	1.76 kg m^2
Inertia constant	H	2.5
Governor time constant	τ_g	0.25 s
Frequency droop coefficient	k_f	$2S/(0.03 n_p f_m)$
Damping coefficient	k_p	8×10^{-5}
Voltage droop coefficient	k_v	$S/(0.03 V_{\mathrm{gH}})$
Exciter integral gain	k_q	1.16
Base impedance	Z_{base}	V_{gH}^2/S
Armature resistance	R_a	$0.02 Z_{\mathrm{base}}$
Synchronous inductance	L_s	$0.6 Z_{\mathrm{base}}/\omega$

VIII. Conclusion

A new inverter control approach for a class of current-control based grid-connected inverters is introduced in this paper. The performance of the proposed controller is compared with that of conventional controller approaches, and based on that, design guidelines are presented. The objective of the controller is to operate the inverter robustly during weak grid conditions. The destabilizing effect of PLL dynamics on controller performance is substantially reduced by including the PLL state variables among the entire system state and use them to optimally generate the control input.

Grid distortions and their crucial impact on the inverter power quality degradation is also considered in this study. It is shown that the introduced controller inherently improves the power quality aspects. This paper further introduced a methodology to feed forward an error term from the PLL to the current controller in order to enhance the power quality aspects.

Appendix

Modeling of 3-phase synchronous generator

Mathematical model for 3-phase synchronous generator is developed as shown in Fig. 28. The parameters used in modeling are listed in Table III.

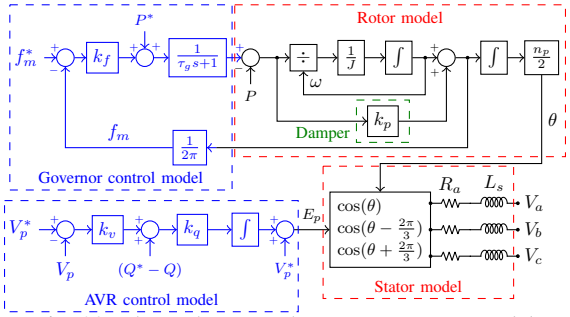

Fig. 28: Three-phase synchronous generator model

References

[1] "IEEE application guide for IEEE Std. 1547(TM), IEEE standard for interconnecting distributed resources with electric power systems," *IEEE Std 1547.2-2008*, pp. 1–217, April 2009.

[2] UL1741 Standard, "Standard for inverters, converters, controllers and interconnection system equipment for use with distributed energy resources," Jan 2010.

[3] California Public Utility Commission, "Rule 21 interconnection," July 2017.

[4] IEEE/NERC Task Force on Short-Circuit and System Performance Impact of Inverter Based Generation, Technical Report PES - TR68, "Impact of inverter based generation on bulk power system dynamics and short-circuit performance," July 2018.

[5] L. Yang, Z. Chen, X. Zhou, W. Wu, W. Tan, J. Guerrero *et al.*, "Effect of phase locked loop on small-signal perturbation modeling and stability analysis for three-phase LCL-type inverter connected to weak grid," *IET Renewable Power Generation*, 2018.

[6] D. Yang, X. Ruan, and H. Wu, "Impedance shaping of the grid-connected inverter with LCL filter to improve its adaptability to the weak grid condition," *IEEE Transactions on Power Electronics*, vol. 29, no. 11, pp. 5795–5805, 2014.

[7] Y. Huang, X. Yuan, J. Hu, P. Zhou, and D. Wang, "DC-bus voltage control stability affected by AC-bus voltage control in VSCs connected to weak AC grids," *IEEE Journal of Emerging and Selected Topics in Power Electronics*, vol. 4, no. 2, pp. 445–458, 2016.

[8] M. Davari and Y. A.-R. I. Mohamed, "Robust vector control of a very weak-grid-connected voltage-source converter considering the phase-locked loop dynamics," *IEEE Transactions on Power Electronics*, vol. 32, no. 2, pp. 977–994, 2017.

[9] V. Diedrichs, A. Beekmann, K. Busker, S. Nikolai, and S. Adloff, "Control of wind power plants utilizing voltage source converter in high impedance grids," in *Power and Energy Society General Meeting*. IEEE, 2012, pp. 1–9.

[10] T. Midtsund, J. Suul, and T. Undeland, "Evaluation of current controller performance and stability for voltage source converters connected to a weak grid," in *2nd International Symposium on Power Electronics for Distributed Generation Systems (PEDG)*. IEEE, 2010, pp. 382–388.

[11] N. P. Strachan and D. Jovcic, "Stability of a variable-speed permanent magnet wind generator with weak AC grids," *IEEE Transactions on Power Delivery*, vol. 25, no. 4, pp. 2779–2788, 2010.

[12] D. Dong, B. Wen, D. Boroyevich, P. Mattavelli, and Y. Xue, "Analysis of phase-locked loop low-frequency stability in three-phase grid-connected power converters considering impedance interactions," *IEEE Transactions on Industrial Electronics*, vol. 62, no. 1, pp. 310–321, 2015.

[13] T. Ackermann, *Wind power in power systems*. John Wiley & Sons, 2005.

[14] Z. Ye, R. Walling, L. Garces, R. Zhou, L. Li, and T. Wang, "Study and development of anti-islanding control for grid-connected inverters," National Renewable Energy Lab., Golden, CO (US), Tech. Rep., 2004.

[15] M. F. M. Arani and Y. A.-R. I. Mohamed, "Analysis and performance enhancement of vector-controlled VSC in HVDC links connected to very weak grids," *IEEE Transactions on Power Systems*, vol. 32, no. 1, pp. 684–693, 2017.

[16] Y. Huang, X. Yuan, J. Hu, and P. Zhou, "Modeling of VSC connected to weak grid for stability analysis of DC-link voltage control," *IEEE Journal of Emerging and Selected Topics in Power Electronics*, vol. 3, no. 4, pp. 1193–1204, 2015.

[17] A. Akhavan, H. R. Mohammadi, and J. M. Guerrero, "A comprehensive control system for multi-parallel grid-connected inverters with LCL filter in weak grid condition," *Electric Power Systems Research*, vol. 163, pp. 288–300, 2018.

[18] Z. Xiao, M. Zhu, Y. Huang, J. M. Guerrero, and J. C. Vasquez, "Coordinated primary and secondary frequency support between microgrid and weak grid," *IEEE Transactions on Sustainable Energy*, 2018.

[19] M. K. Ghartemani, S. A. Khajehoddin, P. K. Jain, and A. Bakhshai, "Problems of startup and phase jumps in PLL systems," *IEEE Transactions on Power Electronics*, vol. 27, no. 4, pp. 1830–1838, 2012.

[20] F. Gonzalez-Espin, G. Garcerá, I. Patrao, and E. Figueres, "An adaptive control system for three-phase photovoltaic inverters working in a polluted and variable frequency electric grid," *IEEE Transactions on Power Electronics*, vol. 27, no. 10, pp. 4248–4261, 2012.

[21] K.-J. Lee, J.-P. Lee, D. Shin, D.-W. Yoo, and H.-J. Kim, "A novel grid synchronization PLL method based on adaptive low-pass notch filter for grid-connected PCS," *IEEE Transactions on Industrial Electronics*, vol. 61, no. 1, pp. 292–301, 2014.

[22] Z. Ali, N. Christofides, L. Hadjidemetriou, E. Kyriakides, Y. Yang, and F. Blaabjerg, "Three-phase phase-locked loop synchronization algorithms for grid-connected renewable energy systems: A review," *Renewable and Sustainable Energy Reviews*, vol. 90, pp. 434–452, 2018.

[23] C. Zhang, X. Wang, and F. Blaabjerg, "Analysis of phase-locked loop influence on the stability of single-phase grid-connected inverter," in

6th International Symposium on Power Electronics for Distributed Generation Systems (PEDG). IEEE, 2015, pp. 1–8.

[24] J. Z. Zhou, H. Ding, S. Fan, Y. Zhang, and A. M. Gole, "Impact of short-circuit ratio and phase-locked-loop parameters on the small-signal behavior of a VSC-HVDC converter," *IEEE Transactions on Power Delivery*, vol. 29, no. 5, pp. 2287–2296, 2014.

[25] J. A. Suul, S. D'Arco, P. Rodriguez, and M. Molinas, "Extended stability range of weak grids with voltage source converters through impedance-conditioned grid synchronization," IET 2015.

[26] A. A. A. Radwan and Y. A.-R. I. Mohamed, "Improved vector control strategy for current-source converters connected to very weak grids," *IEEE Trans on Power Systems*, vol. 31, no. 4, pp. 3238–3248, 2016.

[27] C. Guo, W. Liu, C. Zhao, and R. Iravani, "A frequency-based synchronization approach for the VSC-HVDC station connected to a weak AC grid," *IEEE Transactions on Power Delivery*, vol. 32, no. 3, pp. 1460–1470, 2017.

[28] L. Zhang, L. Harnefors, and H.-P. Nee, "Power-synchronization control of grid-connected voltage-source converters," *IEEE Transactions on Power Systems*, vol. 25, no. 2, pp. 809–820, 2010.

[29] M. Karimi-Ghartemani, "Linear and pseudolinear enhanced phased-locked loop (EPLL) structures," *IEEE Transactions on Industrial Electronics*, vol. 61, no. 3, pp. 1464–1474, 2014.

[30] M. Castilla, J. Miret, J. Matas, L. G. De Vicuňa, and J. M. Guerrero, "Control design guidelines for single-phase grid-connected photovoltaic inverters with damped resonant harmonic compensators," *IEEE Transactions on Industrial Electronics*, vol. 56, no. 11, pp. 4492–4501, 2009.

[31] S. Silwal and M. Karimi-Ghartemani, "On the design of proportional resonant controllers for single-phase grid-connected inverters," in *12th International Conference on Control and Automation (ICCA)*. IEEE, 2016, pp. 797–803.

[32] S. A. Khajehoddin, M. Karimi-Ghartemani, and M. Ebrahimi, "Optimal and systematic design of current controller for grid-connected inverters," *IEEE Journal of Emerging and Selected Topics in Power Electronics*, 2017.

[33] M. Karimi-Ghartemani, S. A. Khajehoddin, P. Jain, and A. Bakhshai, "Linear quadratic output tracking and disturbance rejection," *International Journal of Control*, vol. 84, no. 8, pp. 1442–1449, 2011.

[34] S. Khajehoddin, M. Karimi-Ghartemani, A. Bakhshai, and P. Jain, "High quality output current control for single phase grid-connected inverters," in *Twenty-Ninth Annual IEEE Applied Power Electronics Conference and Exposition (APEC)*. IEEE, 2014, pp. 1807–1814.

[35] M. Karimi-Ghartemani, *Enhanced phase-locked loop structures for power and energy applications*. John Wiley & Sons, 2014.

Sushil Silwal (S'15) received his B.Tech. degree in Electrical Engineering from Motilal Nehru National Institute of Technology (MNNIT), India, in 2012, and worked in Bombardier Transportation Limited, a multinational railway venture, until 2014 as an Assistant Manager/Engineer in three different departments: Engineering, Product Introduction, and Propulsion Converter Control. He is currently working towards his Ph.D. degree in the control of renewable and distributed energy resources from Department of Electrical and Computer Engineering at Mississippi State University, USA. His research interests include control of power electronic converters, renewable energy integration, and control & stability analysis of power system in general.

Seyedfoad Taghizadeh received his M.Sc. degree in Electrical and Electronic Engineering from the Universiti Tenaga Nasional (UNITEN), Malaysia, in 2013. He received the Ph.D. degree in Electrical Engineering from the Macquarie University, Australia in 2018. He is currently working as a Research Fellow in the School of Engineering, Macquarie University, Australia. His research interests include electric vehicle chargers, control systems, renewable energy integration, power quality, and energy storage systems

Masoud Karimi Ghartemani (SM'09) received his Ph.D. degree in Electrical and Computer Engineering from the University of Toronto, Canada, in 2004. Subsequently, he worked at Sharif University of Technology, Tehran, and Queen's University, Ontario, before joining the Department of Electrical and Computer Engineering at the Mississippi State University, USA, in 2012 as an associate professor. His general research area is power systems analysis, stability, and control. His particular interest is in the integration of distributed and renewable energy systems and the modeling and control of such systems at high level of deployment in the electric grid.

M. Jahangir Hossain (M'10-SM'13) received the B.Sc. and M.Sc. Eng. degrees from Rajshahi University of Engineering and Technology (RUET), Bangladesh, in 2001 and 2005, respectively, and the Ph.D. degree from the University of New South Wales, Australia, all in electrical and electronic engineering. He is currently an Associate Professor with the Department of Engineering, Macquarie University. Before joining there, he served as a Senior Lecture and a Lecturer in the Griffith School of Engineering, Griffith University, for five years and as a Research Fellow in the School of Information Technology and Electrical Engineering, University of Queensland, Brisbane, Australia. His research interests include renewable energy integration and stabilization, voltage stability, micro grids and smart grids, robust control, electric vehicles, flexible ac transmission systems devices, and energy storage systems.

Masoud Davari (S'08–M'17) was born in Isfahan, Iran, on September 14, 1985. He received the B.Sc. degree (with Distinction) in electrical engineering-power from the Isfahan University of Technology, Isfahan, Iran, in September 2007, the M.Sc. degree (with Distinction) in electrical engineering-power from Amirkabir University of Technology-Tehran Polytechnic, Tehran, Iran, in January 2010, and the Ph.D. degree in electrical engineering-energy systems from the University of Alberta, Edmonton, AB, Canada, in January 2016.

He has been working with Iran's Grid Secure Operation Research Center and Iran's Electric Power Research Institute (EPRI) in Tehran, Iran, from January 2010 to December 2011. From April 2015 to June 2017, he has been collaborating with Quanta-Technology Company in the field of the dynamic interaction of renewable energy systems with smart grids as well as control, protection, and automation of microgrids as a Senior R & D Specialist and Senior Consultant. Afterward, since July 2017, he has joined the Department of Electrical and Computer Engineering in Allen E. Paulson College of Engineering and Computing at Georgia Southern University, Statesboro, GA, USA as a tenure-track Assistant Professor faculty member. His research interests include the dynamics, controls, and protections of different types of power electronic converters, which are employed in the hybrid ac/dc smart grids, and hardware-in-the-loop (HIL) testing of modernized power systems.

Dr. Davari is an invited member of the Golden Key International Honour Society. He is an active member and a chapter lead (for Chapter 3) in the IEEE WG P2004, a newly established IEEE working group on the Hardware-In-the-Loop (HIL) simulation for IEEE Standards Association, from June 2017 until now. He served as the chair of the Literature Review Subgroup of DC@home Standards for IEEE Standards Association from April 2014 to October 2015. He has developed and implemented several experimental test rigs for both research universities and the industry. He is also the author, the invited reviewer, and the invited speaker of several IEEE Transactions and journals, IET journals, Energies journal, various conferences, and diverse universities and places from different societies.